



Friction stir welding of as-extruded Mg–Al–Zn alloy with higher Al content. Part I: Formation of banded and line structures

J. Yang, D.R. Ni, D. Wang, B.L. Xiao, Z.Y. Ma*

National Laboratory for Materials Science, Institute of Metal Research, Chinese Academy of Sciences, 72 Wenhua Road, Shenyang 110016, China

ARTICLE INFO

Article history:

Received 4 April 2014

Received in revised form 30 July 2014

Accepted 1 August 2014

Available online 2 August 2014

Keywords:

Magnesium alloys

Friction stir welding

Banded structure

Line structure

Mechanical properties

ABSTRACT

6-mm-thick extruded Mg–Al–Zn (AZ80) alloy plates were subjected to friction stir welding at a welding speed of 100 mm·min⁻¹ and tool rotation rates of 400–1200 rpm, and the highest joint efficiency of 92% was achieved at 800 rpm. Friction stir welding resulted in the dissolution of coarse β -Mg₁₇Al₁₂ particles, with fewer and smaller β particles distributed at the grain boundaries in the nugget zones; meanwhile, banded structures resulting from different Al concentrations were observed in the nugget zones. As the rotation rate increased, the grain size of the nugget zones increased, but the β particles showed little variation in the quantity and size. At low rotation rates, uniform microstructures were produced in the joints, and during tensile testing the joints failed in the nugget zones where was the lowest hardness region of the joints. However, a line structure containing the β particles was observed at the boundary of the nugget zone at the highest rotation rate, which resulted in a decrease in the tensile properties. The results indicated that higher rotation rates would not be suitable for the friction stir welding of wrought Mg–Al–Zn alloys with higher Al content.

© 2014 Elsevier Inc. All rights reserved.

1. Introduction

Mg alloys are very attractive in structural applications of aerospace and automobile industries for weight reduction and energy saving. The structural application of Mg alloys inevitably involves welding and joining during manufacturing. However, defects such as porosity, thermal cracks, and oxidization often occur in the fusion welding of Mg alloys.

As a novel solid-state joining technique, friction stir welding (FSW) can effectively avoid the drawbacks of the fusion welding and has been successfully used for welding Al alloys [1]. Although Mg alloys show poor deformability at room temperature, the deformability would be greatly improved at high temperatures for the activation of non-basal slips [2], and this is important for the FSW. By altering welding parameters such as pin and shoulder sizes, welding speed (v), and rotational rate (ω), high-quality FSW joints can be obtained. Recently, FSW has been successfully used to join various Mg alloys, such as Mg–Al–Zn, Mg–Al–Mn, Mg–Al–Ca, Mg–Zn–Zr, and Mg–Zn–Y–Zr [3–18].

Among various kinds of Mg alloys, AZ series alloys were the most fully developed and widely used in manufacturing production for low cost and good properties. For the AZ series alloys, most FSW studies were focused on lower Al content alloys, such as AZ31 and AZ61 [3–9]. It was reported that increasing FSW heat input such as the tool shoulder diameter and the rotation rate could increase the tensile

strength of FSW AZ31 joints [3,19]. At tool rotation rate as high as 3500 rpm, a joint efficiency as high as 95% was achieved in the FSW AZ31 joint. This phenomenon is quite different from that observed in FSW Al alloy joints [1]. Besides, much research has been focused on the deformation behaviors of FSW joint, and basal slip and twinning have been proven to be the main deformation mechanism [19,20].

By comparison, FSW studies of the Mg alloys with higher Al content (AZ80 and AZ91) are limited with the main focus on the as-cast alloys which exhibited low strength and ductility due to the coarse grains and coarse network grain boundary β phase (Mg₁₇Al₁₂) [10–12,21]. It was reported that FSW could effectively dissolve the coarse eutectic β phase and refine the grains in cast AZ91D alloy with the hardness of the nugget zone (NZ) increased greatly [10]. Thus, the FSW joint of as-cast AZ91 alloy could show a similar UTS to that of the parent material (PM) [11].

However, for the wrought (rolled or extruded) Mg alloys with higher Al content, their strength and ductility are significantly improved due to smaller grains and fewer coarse β phases [22]. In this case, the weldability, the mechanical properties and fracture behavior of resultant FSW joints might be quite different from those of the as-cast counterparts. However, investigation in this aspect is lacking.

The present investigation aims to (a) study the effect of FSW parameters on microstructures and tensile properties of the Mg–Al–Zn alloy with high Al content and (b) evaluate the effect of the β precipitates on the weld properties of this alloy. Part I is presented in this article, while Part II will be described in a companion article.

In this article, as-extruded AZ80 plates were subjected to FSW investigation in a wide tool rotation rate range of 400–1200 rpm at a constant

* Corresponding author.

E-mail address: zym@imr.ac.cn (Z.Y. Ma).

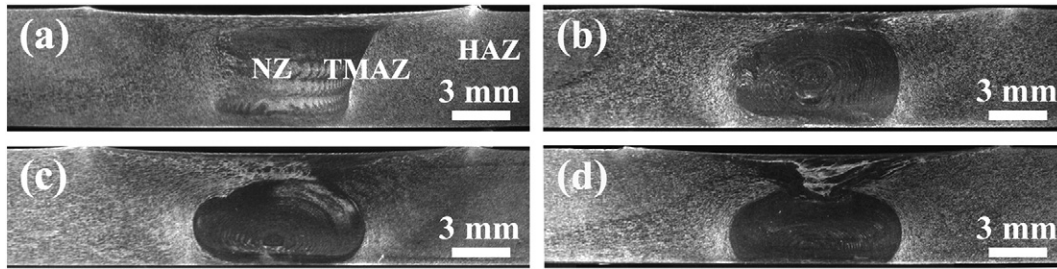


Fig. 1. Cross-sectional macrographs of FSW AZ80 joints at different rotation rates: (a) 400 rpm, (b) 600 rpm, (c) 800 rpm, and (d) 1200 rpm (the advancing side is on the right).

traverse speed of $100 \text{ mm} \cdot \text{min}^{-1}$. The aim is to (a) establish the process window for FSW of as-extruded AZ80 alloy and (b) understand the effect of tool rotation rate on the microstructure evolution and mechanical behavior of FSW AZ80 joints.

2. Material and Methods

AZ80 extruded plates with a nominal composition of 8.00Al–0.33Zn–0.25Mn–0.036Si–0.0018Cu–0.0012Ni–0.0016Fe (in wt.%) were used in this study. 6-mm-thick plates were friction stir welded along the extrusion direction at a traverse speed of $100 \text{ mm} \cdot \text{min}^{-1}$ and tool rotation rates of 400, 600, 800, and 1200 rpm, respectively. A tool with a concave shoulder 20 mm in diameter and a threaded conical pin 8 mm in root diameter, 6.2 mm in tip diameter and 5.7 mm in length was used. The FSW was performed under the plunge control model with the plunge depth being fixed at 0.15 mm with a tilt angle of 2.7° for all the welding parameters. The tool was carefully machined and mounted to reduce the eccentricity as much as possible.

The specimens for microstructural examinations were cross-sectioned perpendicular to the welding direction. Microstructural characterization and analysis were carried out via optical microscopy (OM), scanning electron microscopy (SEM), and transmission electron microscopy (TEM). The specimens for OM and SEM observations were prepared by mechanical polishing and etching using a solution of 4.2 g picric acid, 10 ml acetic acid, 70 ml ethanol, and 10 ml water. Thin foils for TEM were prepared by the ion-milling technique. The grain size was measured using the linear intercept method with the measuring direction perpendicular to both the normal and welding directions.

Vickers hardness and tensile tests were conducted in accordance with ASTM: E384-11e1 and ASTM: E8/E8M-11, respectively. The hardness of the welds was measured along the mid-thickness of the plates with a 300 g load for 10 s using a LECO-LM247AT type Vickers-hardness tester. Transverse tensile specimens with a gauge length of 50 mm and width of 10 mm were machined perpendicular to the FSW direction with the NZ in the center of the gauge. Tensile tests were conducted at a strain rate of $1 \times 10^{-3} \text{ s}^{-1}$ with a Zwick Z050 tester at room temperature. The tensile properties of each FSW joint reported

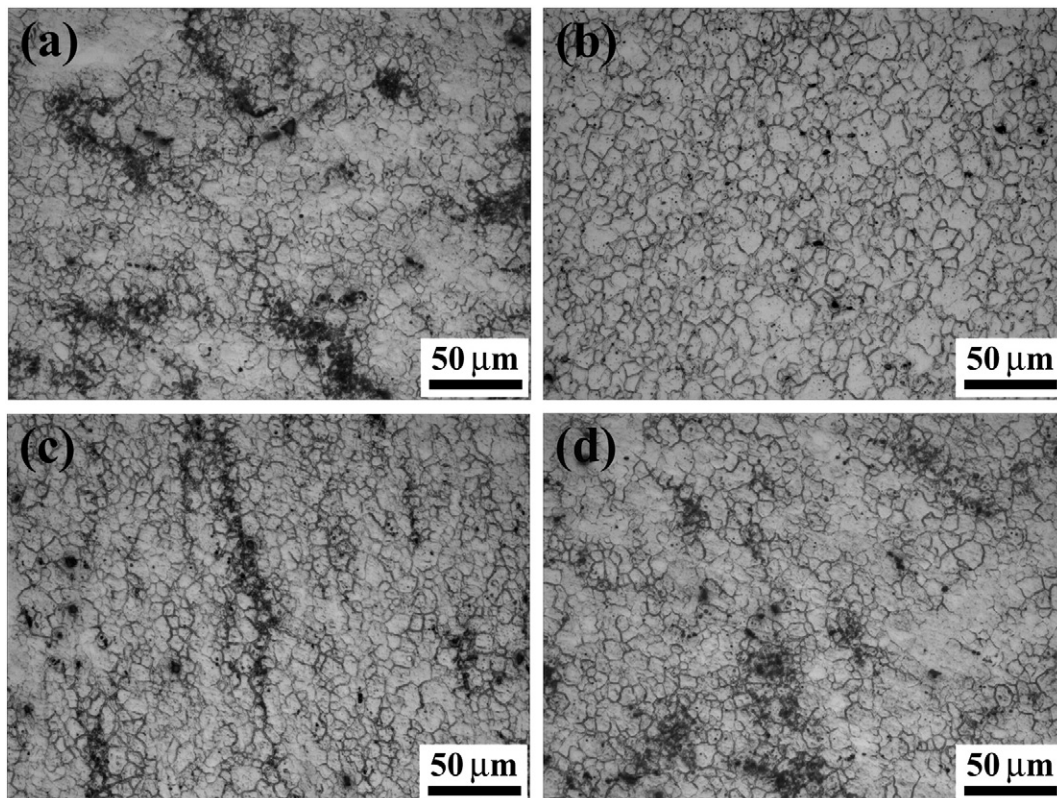


Fig. 2. OM microstructures of FSW AZ80 joint at 400 rpm: (a) PM, (b) NZ, (c) TMAZ, and (d) HAZ.

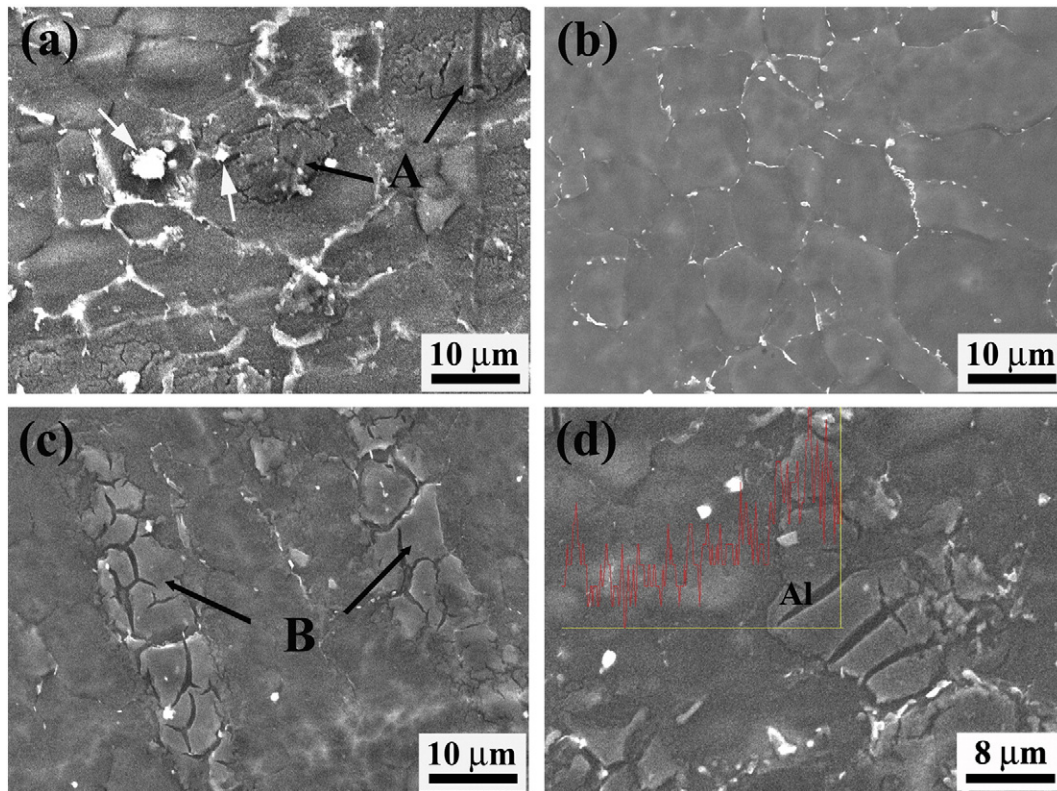


Fig. 3. SEM images of FSW AZ80 joint at 400 rpm: (a) PM, (b) NZ, (c) TMAZ, and (d) EDS line scan of Al content from heterogeneous structure to matrix in TMAZ.

were the averages of three test results. The fracture surfaces were examined using SEM.

3. Results and Discussion

3.1. Microstructural Characteristics

3.1.1. Microstructures in different zones

Fig. 1 shows the cross-sectional macrographs of FSW AZ80 joints at various rotation rates. No obvious defects were found in these joints and three microstructural zones were identified in the cross sections of the joints, i.e. NZ, thermo-mechanically affected zone (TMAZ), and heat-affected zone (HAZ). The lower rotation rate of 400 rpm produced a basin-shaped NZ (Fig. 1a). When increasing the rotation rate the NZ changed from a basin shape to an elliptical one (Fig. 1b–d); however, the elliptical NZ became small and the shoulder affected region enlarged at 1200 rpm (Fig. 1d). These macrographs showed that the nugget shapes of the FSW AZ80 were apparently parameter dependent. This was attributed to the different material flow forms at different rotation rates [23], and a similar result was also reported in the FSW Al alloys [24].

The PM showed an inhomogeneous fine-grained microstructure characterized by equiaxed grains with an average size of 16.2 μm and some heterogeneous structures (black regions in Fig. 2a). For the FSW joint at 400 rpm, equiaxed grains with an average grain size of 14.4 μm were observed in the NZ (Fig. 2b). In the TMAZ, some heterogeneous structures were found to be distributed along the normal direction (Fig. 2c). The microstructure in the HAZ was similar to that in the PM (Fig. 2d).

SEM observations showed a bright contrast of β phase, dark contrast of α -Mg matrix, and severely-corroded regions (area A) in the PM (Fig. 3a) with a large number of coarse eutectic β particles distributed at the grain boundaries. Besides, some coarse particles (as shown by white arrows) were also observed, which is a binary compound of Al and Mn [25]. Energy dispersive spectroscopic (EDS) analyses indicated

that the Mg matrix contained more than 6.1 wt.% Al. The severely-corroded regions were found to be the heterogeneous structures in the OM photograph and contained 21.2 wt.% Al, which was much higher than the maximum solubility of Al in Mg (12.5 wt.%) but lower than that in the β phase (40 wt.%). Therefore, the heterogeneous structures were a kind of the supersaturated solid solution zone which was considered as the non-equilibrium eutectic constituent in the as-cast Mg–Al–Zn alloys with higher Al content [26,27]. In the present study, the AZ80 cast billet was directly extruded without a full pre-homogenization; therefore, the heterogeneous structures (supersaturated solid solution zone) still remained after extrusion.

SEM observations also showed that most of the β particles in the region of the NZ and TMAZ were dissolved into the matrix (Fig. 3b and c). The average Al content in the matrix of the NZ was about 7.5 wt.%, higher than that in the PM. In the TMAZ, the heterogeneous structures (area B) were still observed and contained 15.7 wt.% Al (Fig. 3c), which was lower than that in area A of the PM. The EDS line scan profile showed that the Al content decreased from the heterogeneous structures to the Mg matrix (Fig. 3d). The distribution of the β particles in the HAZ (not shown) was similar to that in the PM, but a lower Al content (about 18.9 wt.%) in the heterogeneous structures was detected in the HAZ.

During the FSW process, severe shear deformation significantly accelerated the Al–Mg interdiffusion rate and shortened the diffusion distance [28]. In this case, most β was dissolved and large particles were refined in the welds. However, the different deformation degrees and temperatures changed the Al content in the NZ, TMAZ, and HAZ. The NZ underwent the highest deformation degree and temperature, therefore the Mg matrix contained more Al than in the PM. However, both

Table 1

Grain size in nugget zone of FSW AZ80 joints at various rotation rates.

ω , rpm	400	600	800	1200	PM
d_{nugget} , μm	12.1	13.5	14.4	30.9	16.2

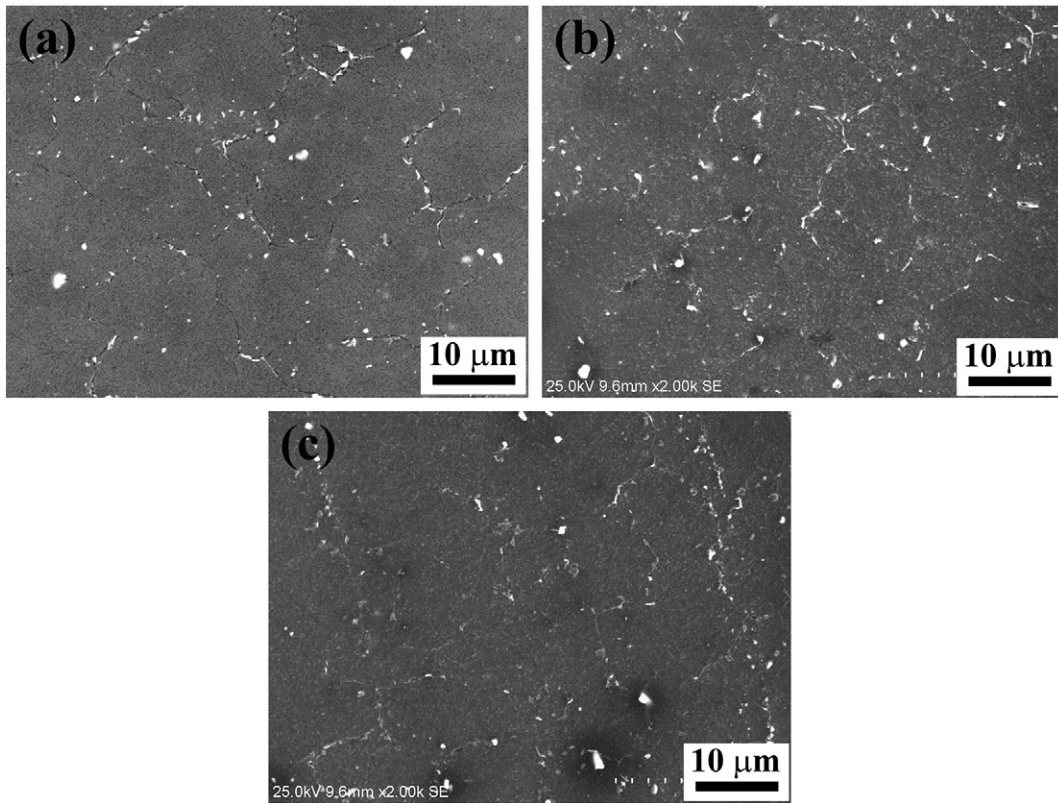


Fig. 4. SEM images of NZs in FSW AZ80 joints at different rotation rates: (a) 600 rpm, (b) 800 rpm, and (c) 1200 rpm.

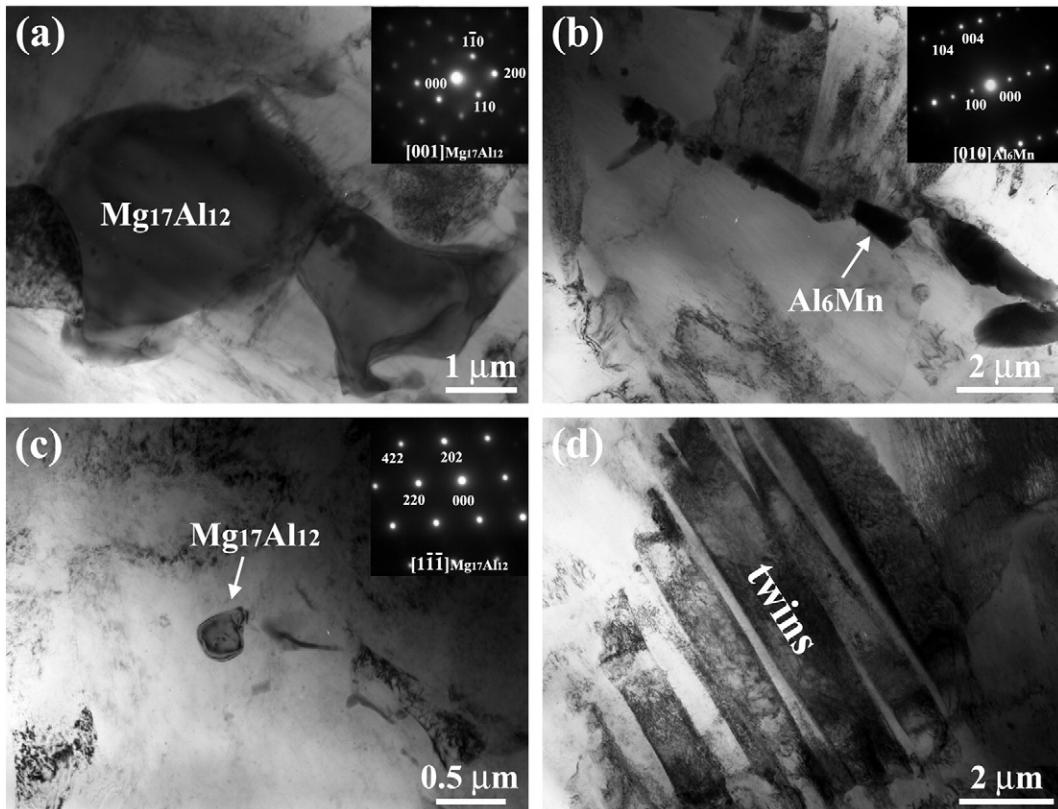


Fig. 5. TEM images showing: (a) and (b) compounds in grain boundary of PM; (c) retained $Mg_{17}Al_{12}$ and (d) Mg twins in NZ of FSW joint.

the temperature and deformation degree were lower in the TMAZ, leading to the incomplete diffusion of Al. Consequently, the heterogeneous structures in the TMAZ were detected to have lower Al content than those in the PM. Meanwhile, the material in the TMAZ was elongated along the rotational direction [23], making the heterogeneous structures distributed along the normal direction (Figs. 2c and 3c). Because only lower heat input played a role in the HAZ, the grain size and distribution of β in the HAZ had little difference from those in the PM (Fig. 2d), with a lower Al content in the heterogeneous structures.

As the rotation rate increased from 400 to 800 rpm, the grain size of the NZ slightly increased, but it was still smaller than that of the PM (Table 1); however, at 1200 rpm larger grains ($30.9\ \mu\text{m}$) were generated. It was found that fewer and smaller β particles were distributed at the grain boundaries in the NZ than in the PM (Figs. 3b and 4). Generally, the temperature in the NZ increased with the rotation rate [29] and this resulted in a corresponding increase in the grain size. The temperature of the NZ was reported to be between $340\ ^\circ\text{C}$ and $500\ ^\circ\text{C}$ in the FSW Mg alloy [10], which was close to the melting point of the β . However, the number of the β phase showed little variation with the rotation rate (Figs. 3b and 4). This is mainly attributed to the fact that the duration of dissolution for second phase particles was similar at various rotation rates when the welding speed was constant [30]. Thus, similar dissolution degrees of the β phase were observed at different rotation rates.

Fig. 5 shows the TEM microstructure of the PM and the NZ at 800 rpm. Coarse β - $\text{Mg}_{17}\text{Al}_{12}$ and blocky Al_6Mn compound particles were observed at the grain boundaries of the PM (Fig. 5a and b). After FSW most of the β and Al_6Mn particles disappeared with only a few small particles being observed, indicating that FSW effectively broke up and/or dissolved those compound particles (Fig. 5c). Meanwhile, deformation Mg twins were observed in the NZ (Fig. 5d), which were generated by the severe plastic deformation resulting from the rotating tool.

3.1.2. Banded structure in NZ

As shown in Fig. 1, a banded structure was observed in the NZs at various rotation rates. Fig. 6 shows the magnified images of the banded structure in the NZ at 800 rpm. The bands are shown to result from alternating regions of heterogeneous structures (Fig. 6b). EDS analyses indicated that the Al content in the heterogeneous structures (points 1–6, averaged 10.1 wt.%) was higher than that in the heterogeneous-structure-free zones (points 7–12, averaged 6.2 wt.%). The bands with higher Al concentrations were the severely-corroded regions and the dark bands in Fig. 6a. It was reported that the regions with different Al contents had different etching reactions in the AZ91 [26]. Furthermore, as shown in Fig. 6b and c, the β particles were distributed at the grain boundaries in both the heterogeneous structures and other regions, with AlMn compound particles in the grains. Therefore, it is concluded that the different bands with different etching reactions resulted from different Al concentrations.

This phenomenon was similar to the banded structure resulting from the particle-rich bands in FSWed 2024-T3 Al alloy: the uniform distribution of particles in the PM was converted to accumulated particle bands due to the strain gradient in the NZ [31], and the strain gradient on the cross-sectioned plane of the NZ has been confirmed by numerical simulation results [32–34]. The β phase and the heterogeneous structures in the PM of AZ80 were uniformly distributed in this study, which was similar to the hard particle (containing higher concentrations of Cu, Fe, Mg and Mn) distribution in Ref [31]. After FSW, the β phase and the heterogeneous structures could also congregate to form bands in the NZ for the strain gradient. However, different from the undissolved particle, most of the β phases were dissolved and the diffusion of Al atoms occurred in the NZ during FSW. Therefore, it could be inferred that two courses occurred in the NZ during FSW: the dissolution of β phase, and the formation of bands containing the heterogeneous structures and some β phases. The banded structure will be further discussed in Part II.

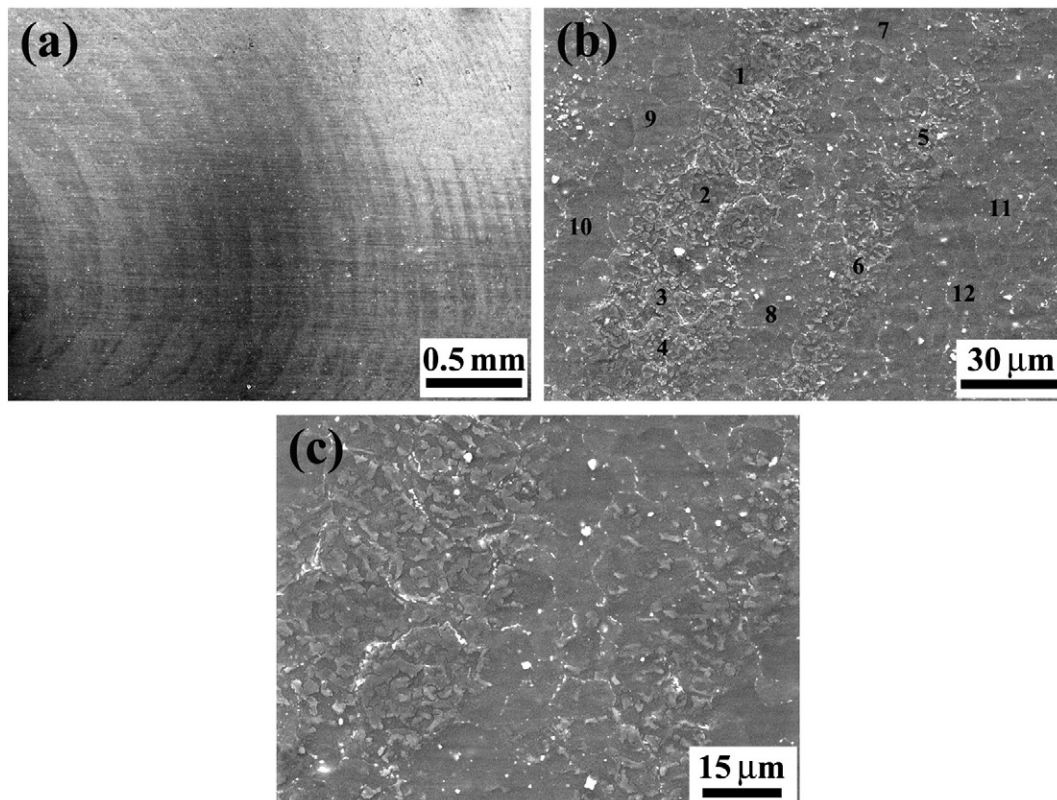


Fig. 6. SEM images showing banded structure in NZ of FSW AZ80 joint at 800 rpm: (a) low magnification, (b) and (c) high magnifications.

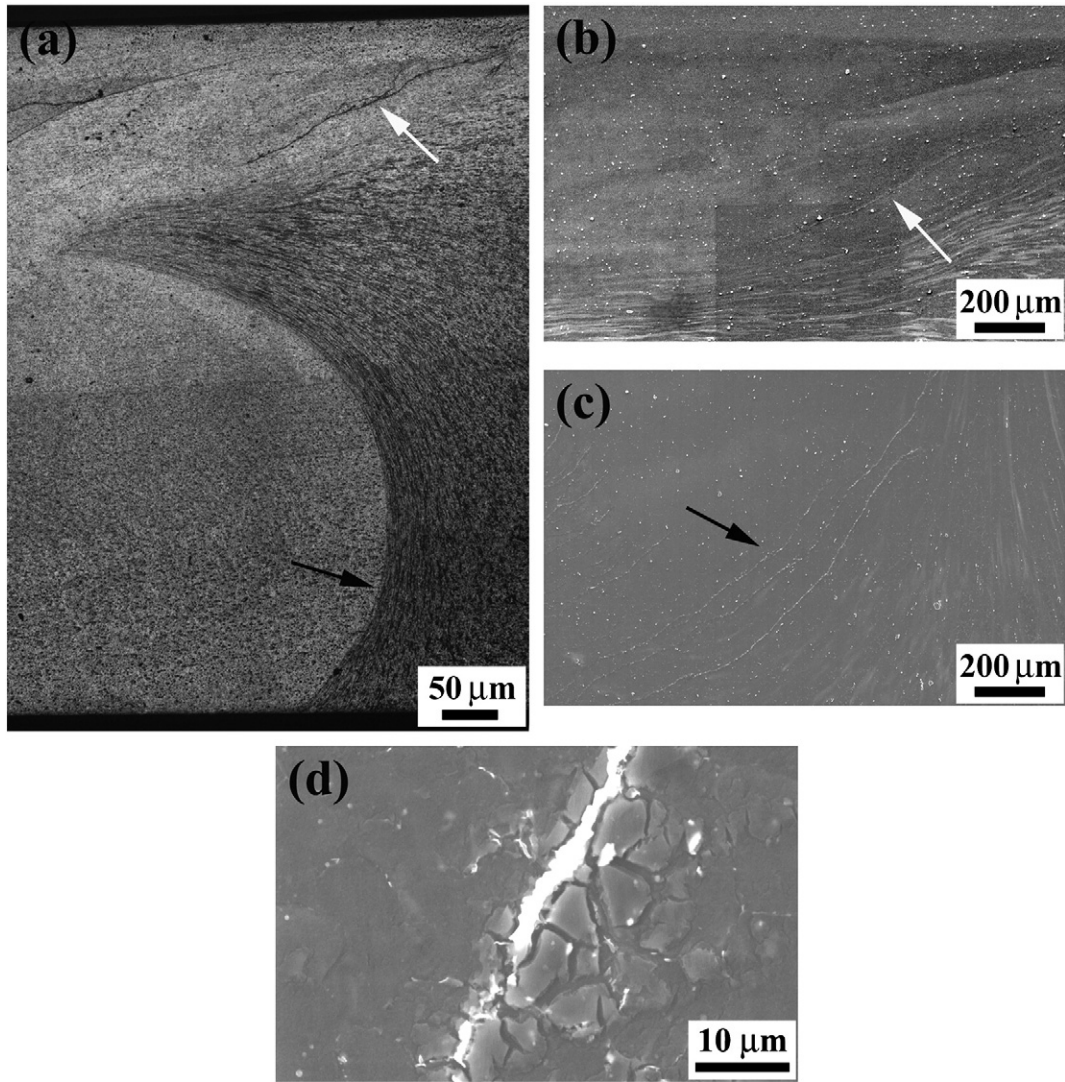


Fig. 7. SEM images of NZ boundary at 1200 rpm: (a) macrograph on advancing side, (b) and (c) line structures as shown by white and black arrows in (a), and (d) magnified image of line structure.

3.1.3. Line Structure

At 1200 rpm, a visible continuous “line structure” was observed at the boundary of the NZ (as shown by arrows in Fig. 7a). The line structure as marked by the white and black arrows is shown in Fig. 7b and c, respectively. The magnification of the line structure shows that a white zone was in the inside of the line structure, while the severely-corroded

zone was in the outside (Fig. 7d). The white zone was determined to be the β phase by EDS.

The formation of the line structure should be related to the material flow during the FSW of AZ80. It was proposed by using finite-element analysis that there existed a certain location where the plastic flow was poor during FSW [35,36], and this region would be the NZ boundary [32]. Meanwhile, the 2D and 3D finite-element simulations showed that the NZ boundary experienced lower strain than the other parts of the NZ [35]. Consequently, the β phase was prone to aggregating at the NZ boundary for the inadequate plastic flow and low strain. Besides, the material flow pattern at a high rotation rate was different from that at a lower one [23], with a smaller region being affected by the pin

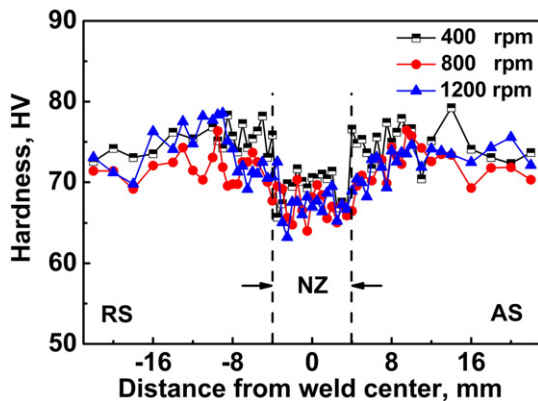


Fig. 8. Hardness profiles of FSW AZ80 joints at various rotation rates. AS: advancing side, RS: retreating side.

Table 2
Tensile properties of FSW AZ80 joints at various rotation rates.

ω , rpm	YS, MPa	UTS, MPa	El. %	Joint efficiency, %	Fracture location
PM	179.4 ± 5.2	330.0 ± 3.4	22.6 ± 0.9	–	–
400	167.0 ± 1.4	291.6 ± 3.9	10.2 ± 0.8	88.4	NZ
600	159.8 ± 1.0	287.3 ± 1.1	8.6 ± 0.4	87.1	NZ
800	160.8 ± 0.5	304.5 ± 1.9	11.5 ± 0.3	92.3	NZ
1200	159.4 ± 0.3	273.7 ± 16	7.2 ± 1.6	82.9	Boundary of NZ

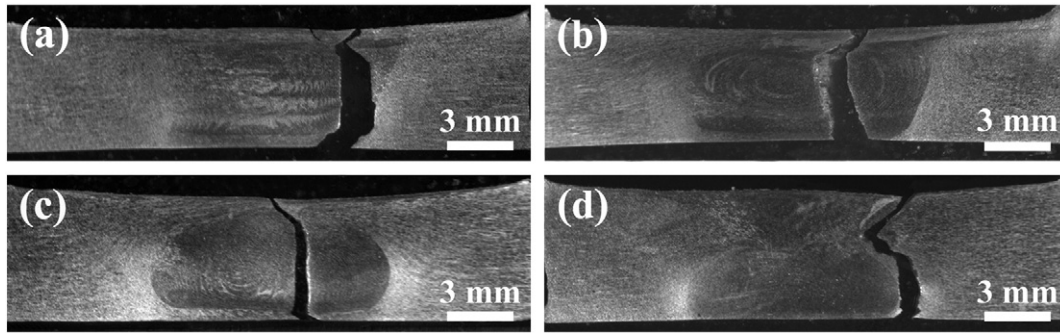


Fig. 9. Macrographs of cross sections of fractured joints at different rotation rates: (a) 400 rpm, (b) 600 rpm, (c) 800 rpm, and (d) 1200 rpm.

rotation. Moreover, a recent study [37] indicated that $Mg_{17}Al_{12}$ phase has a high deformability accompanied by a strong softening during high temperature deformation. Therefore, in the present study, the line structure was found at the NZ boundary at 1200 rpm.

3.2. Microhardness

Fig. 8 shows the hardness profiles of the FSW joints along the mid-thickness at different rotation rates. It can be seen that the hardness profiles were similar for the various FSW joints (400, 800 and 1200 rpm) with the lowest hardness in the NZ. For the FSW joints, the hardness was considered to be affected by the dislocation density, grain size and precipitates.

As shown in Table 1, the grain size in the NZ increased with the rotation rate; in particular, the grain size at 1200 rpm ($30.9 \mu\text{m}$) was larger than that at 400–800 rpm ($12.1\text{--}14.4 \mu\text{m}$). However, the hardness of the NZ had little variation as the rotation rate changed. A similar phenomenon was also observed in the FSW

AZ31, which was attributed to the weak influence of the grain size on the hardness within a certain range [3]. Park et al. [8] reported that there was little variation in the dislocation density between the NZ and PM in FSW AZ61. Besides, it was found that the dislocation density of the NZ in FSW AZ31 varied little with welding parameters [3]. Therefore, the effect of dislocation density on the hardness was not obvious for the FSW AZ series alloys. β was the strengthening phase in the AZ80 alloy. Most of the β phase was dissolved in the NZ during FSW, therefore the NZ exhibited the lowest hardness throughout the whole FSW AZ80 joints.

3.3. Tensile Properties

Table 2 shows the transverse tensile properties of the FSW AZ80 joints. The extruded PM had ultimate tensile strength (UTS) of 330 MPa, yield strength (YS) of 179 MPa, and elongation of 22.6%. Compared to the PM, the FSW joints exhibited decreased UTS, YS, and elongation. The YS of various FSW joints was almost the same, about 90% of the PM. As

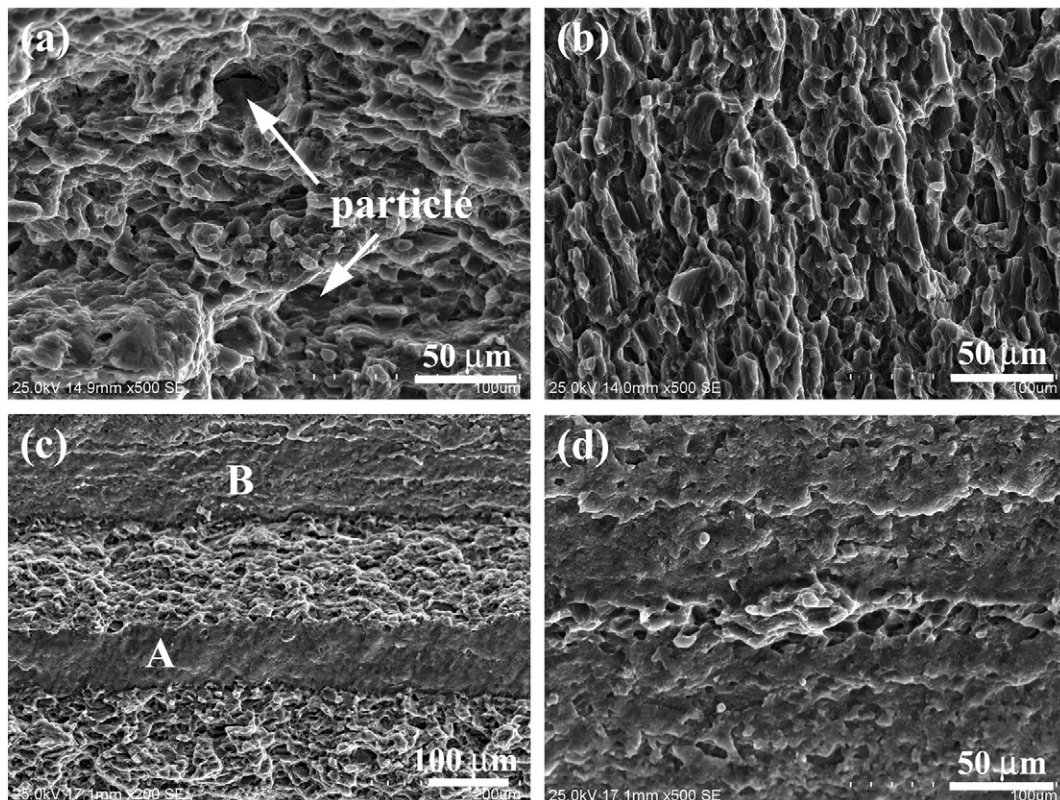


Fig. 10. SEM micrograph of tensile fracture surface of PM and FSW AZ80 joints: (a) PM, (b) 800 rpm, (c) 1200 rpm, and (d) Region B in (c).

the rotation rate increased from 400 to 800 rpm, the UTS of the FSW joints increased; the joints all failed in the NZs (Fig. 9a–c), consistent with the lowest hardness distribution. The maximum joint efficiency of 92% was obtained at 800 rpm. However, the strength of the joint sharply decreased when the rotation rate increased to 1200 rpm, and the failure location shifted to the boundary of the NZ (Fig. 9d).

Fig. 10 shows the SEM fractographs of the PM and FSW joints. For the PM (Fig. 10a), the fracture surfaces were rough and characterized by pits, tearing ridges, and dimples; meanwhile, some cracked particles were found in the bottoms of the pits. The cracked particles indicated that the PM might fail mainly by fracture of the brittle β phases. At 800 rpm (Fig. 10b), the fracture surface of the joint was relatively even and covered with more dimples and tearing ridges, and no cracked particles were visible. This feature was due to the fact that the fracture located in the NZ where most of the β particles were dissolved. By comparison, the joint at 1200 rpm (Fig. 10c) showed a quite different morphology: some smooth stripes (Region A) parallel to the welding direction appeared in the bottom of the weld, and cleavage features were observed on the fracture surface (Region B, Fig. 10d). These special characteristics might result from the material flow at the relatively high rotation rate. During FSW, the material flow varies from the upper to the lower part of the NZ: it is significantly affected by the tool shoulder in the upper part but mainly driven by the tool pin in the lower part [38]. The effect of the tool shoulder is more obvious at the higher rotation rate, and in our previous study a two-layer structured NZ of FSW AZ31 alloy was even formed at an extremely high rotation rate of 3500 rpm [19]. Considering that cracks are likely to generate or propagate along the smooth stripes, they should be partially responsible for the lower strengths and elongation of the FSW joint.

For the FSW joints at 400–800 rpm, the decreased UTS and YS are attributed to the dissolution of the β phases in the NZ and TMAZ, whereas the lower elongation should be due to the nonuniform deformation caused by the special texture distribution [7]. As the rotation rate increased from 400 to 800 rpm, the grain size increased slightly and the distribution of the β phases varied little in the NZs, however, a slight increase in the UTS was detected. A similar result was also observed in the FSW AZ31 [9], in which the increase of the UTS was attributed to the weakening of basal texture when increasing the rotation rate.

The decreased tensile properties of the FSW AZ80 joint at 1200 rpm indicated that the higher rotation rate was unfit for the FSW of extruded AZ80. However, sound FSW AZ31 joints could be achieved at rotation rates ranging from 500 to 3500 rpm [5,6,9,19], which were much wider than those for the AZ80 alloy. Furthermore, our previous study indicated that the joint efficiency of the FSW AZ31 joints increased with increasing the rotation rate from 800 to 3500 rpm [19]. This difference in the weldability between AZ80 and AZ31 should be attributed to the existence of the β phase and higher Al concentration of the Mg matrix in the AZ80 alloy, which significantly decreased the flowability of the Mg matrix, leading to the appearance of the line structure (Fig. 7). It was reported that cracks tended to initiate from the interface of Mg/ β [39] and propagate along the precipitates at the grain boundaries [26]. Therefore, the line structure with coarse β could promote the crack propagation and thus lead to the fracture along the line structure. Consequently, both the strengths and elongation of the FSW AZ80 joint at 1200 rpm obviously decreased.

4. Conclusions

6-mm-thick extruded AZ80 plates were welded by FSW under rotation rates from 400 to 1200 rpm with a traverse speed of $100 \text{ mm} \cdot \text{min}^{-1}$. The following conclusions can be drawn:

- (1) Banded structures were observed in the NZs, which consisted of alternating regions of heterogeneous structures resulting from different Al concentrations. Furthermore, a line structure with the coarse β was detected at the NZ boundary at 1200 rpm.

- (2) The grain size of the NZ increased with the rotation rate. Compared to the PM, fewer and smaller β particles were distributed at the grain boundaries in the NZ and the quantity of β particles exhibited little change with increasing the rotation rate.
- (3) The tensile properties of the FSW joints slightly increased as the rotation rate increased from 400 to 800 rpm with the highest joint efficiency of 92% being obtained at 800 rpm and the fracture occurred in the NZ which exhibited the lowest hardness. However, the joint at 1200 rpm exhibited a reduced strength and elongation with the fracture occurring along the line structure where the coarse β could promote the crack initiation and propagation.

Acknowledgments

This work was supported by the National Natural Science Foundation of China under Grant Nos. 51371179 and 51331008.

References

- [1] R.S. Mishra, Z.Y. Ma, Friction stir welding and processing, *Mater. Sci. Eng. R* 50 (2005) 1–78.
- [2] S.R. Agnew, O. Duygulu, Plastic anisotropy and the role of non-basal slip in magnesium alloy AZ31B, *Int. J. Plast.* 21 (2005) 1161–1193.
- [3] J. Yang, B.L. Xiao, D. Wang, Z.Y. Ma, Effects of heat input on tensile properties and fracture behavior of friction stir welded Mg–3Al–1Zn alloy, *Mater. Sci. Eng. A* 527 (2010) 708–714.
- [4] L. Commin, M. Dumont, J.E. Masse, L. Barrallier, Friction stir welding of AZ31 magnesium alloy rolled sheets: influence of processing parameters, *Acta Mater.* 57 (2009) 326–334.
- [5] M. Abbasi Gharacheh, A.H. Kokabi, G.H. Daneshi, B. Shalchi, R. Sarrafi, The influence of the ratio of “rotational speed/traverse speed” (ω/v) on mechanical properties of AZ31 friction stir welds, *Int. J. Mach. Tools Manuf.* 46 (2006) 1983–1987.
- [6] W.B. Lee, Y.M. Yeon, S.B. Jung, Joint properties of friction stir welded AZ31B–H24 magnesium alloy, *Mater. Sci. Technol.* 19 (2003) 785–790.
- [7] S.H.C. Park, Y.S. Sato, H. Kokawa, Basal plane texture and flow pattern in friction stir weld of a magnesium alloy, *Metall. Mater. Trans. A* 34A (2003) 987–994.
- [8] S.H.C. Park, Y.S. Sato, H. Kokawa, Effect of micro-texture on fracture location in friction stir weld of Mg alloy AZ61 during tensile test, *Scr. Mater.* 49 (2003) 161–166.
- [9] J. Yang, D. Wang, B.L. Xiao, Z.Y. Ma, The microstructure and mechanical properties of friction stir welded Mg–3Al–1Zn alloy at high rotation rates, 8th Inter Friction Stir Welding Symp, Timmendorfer Strand, Germany, 2010.
- [10] S.H.C. Park, Y.S. Sato, H. Kokawa, Microstructural evolution and its effect on Hall–Petch relationship in friction stir welding of thixomolded Mg alloy AZ91D, *J. Mater. Sci.* 38 (2003) 4379–4383.
- [11] W.B. Lee, J.W. Kim, Y.M. Yeon, S.B. Jung, The joint characteristics of friction stir welded AZ91D magnesium alloy, *Mater. Trans.* 44 (2003) 917–923.
- [12] W.P. Xu, L. Xing, L.M. Ke, Analysis of the grain orientation and texture of friction stir welded magnesium alloy, *Mater. Sci. Forum* 620–622 (2009) 97–100.
- [13] G.M. Xie, Z.Y. Ma, L. Geng, Effect of microstructure evolution on mechanical properties of friction stir welded ZK60 alloy, *Mater. Sci. Eng. A* 486 (2008) 49–55.
- [14] J.A. Esparza, W.C. Davis, L.E. Murr, Microstructure–property studies in friction-stir welded, thixomolded magnesium alloy AM60, *J. Mater. Sci.* 38 (2003) 941–952.
- [15] G.M. Xie, Z.Y. Ma, L. Geng, R.S. Chen, Microstructural evolution and mechanical properties of friction stir welded Mg–Zn–Y–Zr alloy, *Mater. Sci. Eng. A* 471 (2007) 63–68.
- [16] D.T. Zhang, M. Suzuki, K. Maruyama, Microstructural evolution of a heat-resistant magnesium alloy due to friction stir welding, *Scr. Mater.* 52 (2005) 899–903.
- [17] G.M. Xie, Z.Y. Ma, L. Geng, Effect of Y addition on microstructure and mechanical properties of friction stir welded ZK60 alloy, *J. Mater. Sci. Technol.* 25 (2009) 351–355.
- [18] G.M. Xie, Z.Y. Ma, L. Geng, Effects of friction stir welding parameters on microstructures and mechanical properties of ZK60 magnesium alloy joints, *Acta Metall. Sin.* 44 (2008) 665–670.
- [19] J. Yang, D. Wang, B.L. Xiao, D.R. Ni, Z.Y. Ma, Effects of rotation rates on microstructure, mechanical properties, and fracture behavior of friction stir-welded (FSW) AZ31 magnesium alloy, *Metall. Mater. Trans. A* 44A (2013) 517–530.
- [20] S. Mironov, Q. Yang, H. Takahashi, I. Takahashi, K. Okamoto, Y.S. Sato, H. Kokawa, Specific character of material flow in near-surface layer during friction stir processing of AZ31 magnesium alloy, *Metall. Mater. Trans. A* 41A (2010) 1016–1024.
- [21] A.H. Feng, B.L. Xiao, Z.Y. Ma, R.S. Chen, Effect of friction stir processing procedures on microstructure and mechanical properties of Mg–Al–Zn casting, *Metall. Mater. Trans. A* 40A (2009) 2447–2456.
- [22] Y. Liu, Y.Y. Li, D.T. Zhang, T.W.L. Ngai, W. Chen, Microstructure and properties of AZ80 magnesium alloy prepared by hot extrusion from recycled machined chips, *Trans. Nonferrous Met Soc. China* 12 (2002) 882–885.
- [23] W.J. Arbegast, A flow-partitioned deformation zone model for defect formation during friction stir welding, *Scr. Mater.* 58 (2008) 372–376.
- [24] Z.Y. Ma, S.R. Sharma, R.S. Mishra, Effect of friction stir processing on the microstructure of cast A356 aluminum, *Mater. Sci. Eng. A* 433 (2006) 269–278.

- [25] A.H. Feng, Z.Y. Ma, Enhanced mechanical properties of Mg–Al–Zn cast alloy via friction stir processing, *Scr. Mater.* 56 (2007) 397–400.
- [26] D.G.L. Prakash, D. Regener, Quantitative characterization of $Mg_{17}Al_{12}$ phase and grain size in HPDC AZ91 magnesium alloy, *J. Alloys Compd.* 461 (2008) 139–146.
- [27] I.A. Yakubtsov, B.J. Diak, C.A. Sager, B. Bhattacharya, W.D. MacDonald, M. Niewczas, Effects of heat treatment on microstructure and tensile deformation of Mg AZ80 alloy at room temperature, *Mater. Sci. Eng. A* 496 (2008) 247–255.
- [28] Z.Y. Ma, A.L. Pilchak, M.C. Juhas, J.C. Williams, Microstructural refinement and property enhancement of cast light alloys via friction stir processing, *Scr. Mater.* 58 (2008) 361–366.
- [29] Ø. Frigaard, Ø. Grong, O.T. Midling, A process model for friction stir welding of age hardening aluminum alloys, *Metall. Mater. Trans. A* 32A (2001) 1189–1200.
- [30] F.C. Liu, Z.Y. Ma, Influence of tool dimension and welding parameters on microstructure and mechanical properties of friction-stir-welded 6061-T651 aluminum alloy, *Metall. Mater. Trans. A* 39A (2008) 2378–2388.
- [31] M.A. Sutton, B. Yang, A.P. Reynolds, R. Taylor, Microstructural studies of friction stir welds in 2024-T3 aluminum, *Mater. Sci. Eng. A* 323 (2002) 160–166.
- [32] S.W. Xu, X.M. Deng, A study of texture patterns in friction stir welds, *Acta Mater.* 56 (2008) 1326–1341.
- [33] Z. Zhang, J.T. Chen, Z.W. Zhang, H.W. Zhang, Coupled thermo-mechanical model based comparison of friction stir welding processes of AA2024-T3 in different thicknesses, *J. Mater. Sci.* 46 (2011) 5815–5821.
- [34] P. Asadi, R.A. Mahdavi, S. Tutunchilar, Simulation and experimental investigation of FSP of AZ91 magnesium alloy, *Mater. Sci. Eng. A* 528 (2011) 6469–6477.
- [35] T. Shinoda, Effect of tool angle on metal flow phenomenon in friction stir welds, *Proc of 3rd Inter Friction Stir Welding Symp.*, Kobe, Japan, 2001.
- [36] S. Lim, S. Kim, C.G. Lee, C.D. Yim, S.J. Kim, Tensile behavior of friction stir welded AZ31-H24 Mg alloy, *Metall. Mater. Trans. A* 36A (2005) 1609–1612.
- [37] J. Ragani, P. Donnadieu, C. Tassin, J.J. Blandin, High temperature deformation of the gamma- $Mg_{17}Al_{12}$ complex metallic alloy, *Scr. Mater.* 65 (2011) 253–256.
- [38] U.F.H.R. Suhuddin, S. Mironov, Y.S. Sato, H. Kokawa, C.W. Lee, Grain structure evolution during friction-stir welding of AZ31 magnesium alloy, *Acta Mater.* 57 (2009) 5406–5418.
- [39] Y.Z. Lu, Q.D. Wang, W.J. Ding, X.Q. Zeng, Y.P. Zhu, Fracture behavior of AZ91 magnesium alloy, *Mater. Lett.* 44 (2000) 265–268.